Utilization of drinking water treatment sludge in concrete paving blocks: Microstructural analysis, durability and leaching properties

Utilization of drinking water treatment sludge in concrete paving blocks: Microstructural analysis, durability and leaching properties

Yue Liu[a], Yan Zhuge[a,*], Christopher W.K. Chow[a,b], Alexandra Keegan[c], Danda Li[a], , Phuong Ngoc Pham[a,d], Jianyin Huang[a,b], Rafat Siddique[e]

[a] *Natural and Built Environments Research Centre, School of Natural and Built Environment, University of South Australia, Adelaide, Australia*
[b] *Future Industries Institute, University of South Australia, Adelaide, Australia*
[c] *Australian Water Quality Centre, South Australian Water Corporation, Adelaide, Australia*
[d] *Faculty of Bridge and Road Engineering, The University of Danang – University of Science and Technology, 54 Nguyen Luong Bang, Danang, Vietnam.*
[e] *Civil Engineering Department, Thapar Institute of Engineering and Technology, Patiala, India*
**Corresponding author. Email address: Yan.Zhuge@unisa.edu.au*

Abstract

The management of abundant drinking water treatment sludge (DWTS) in landfill remains an important issue. The reuse of DWTS as construction material could contribute to the development of greener concrete product and to mitigating the detrimental environment effect from excessive production of DWTS. This paper investigates the potential of using DWTS as sand replacement in Concrete Paving Blocks (CPB). Five CPB mixtures were designed and the replacement ratios of sand by DWTS were 0%, 5%, 10%, 15%, and 20%, by weight. Properties of CPB such as compressive strength, water absorption, abrasion resistance, sulfate attack and metal leachability were determined. The results indicated that above 10% of DWTS, the replacement was detrimental to such properties of the CPB. Microstructure analysis proved the addition of DWTS could result in ettringite formation and the interfacial transition zone (ITZ) between the cement matrix and DWTS was more porous than that of sand. In addition, the metal leachability test of CPB demonstrated that the addition of high-copper DWTS into CPB was safe.

Keywords: Drinking water treatment sludge; Concrete; Paving blocks; Durability properties; Leaching ability; Microstructural analysis.

1. Introduction

Global demand for drinking water has increased dramatically due to rapid population growth and changes in lifestyle, which means water utilities need to produce more drinking water than ever before (Ahmad et al., 2016). The conventional drinking water treatment typically involves several steps, including coagulation-flocculation, sedimentation and filtration. The term 'drinking water treatment sludge (DWTS)' refers to all precipitates or wastes produced during drinking water treatment processes (Ahmad et al., 2016). When aluminium sulfate is used as coagulant for water purification, the acquired DWTS contains high content of Al_2O_3 and SiO_2. In Australia, the DWTS annual production of various water authorities could be up to 43,500 tonnes (Maiden et al., 2015). While in the UK, the annual amount of DWTS in 2014 was reported around 131,000 tonnes (De Carvalho Gomes et al., 2019). Generally, it was estimated that the daily production of DWTS had exceeded 10,000 tonnes on a global scale (Babatunde and Zhao, 2007), which has likely increased in the last decade.

The most common method to deal with DWTS is disposal to landfill. However, landfilling solution has become more difficult and expensive due to the larger amount of DWTS generation, the limited available lands and more stringent environmental laws (Babatunde and Zhao, 2007). For instance, the cost for DWTS disposal exceeded $6.4 million per annum in Victoria, Australia (Maiden et al., 2015) and was £ 5.5 million in the UK (Keeley et al., 2014). Thus, developing new strategies of DWTS management, such as exploring the possibility of using DWTS as a potential construction material, instead of disposal to landfill becomes an urgent need.

DWTS has been used as filler material to produce bricks and ceramic products, due to similar chemical compositions with clay, especially for oxides of silica, aluminium and ferric (Anderson et al., 2003; Benlalla et al., 2015; Huang et al., 2001; Ling et al., 2017; Sarabia et

al., 2019). However, most of studies demonstrated the increase of sludge content decreased the strength and increased water absorption of bricks (Anderson et al., 2003; Huang et al., 2001; Wolff et al., 2015) , e.g. the compressive strength dropped from 17MPa to 7MPa with increasing sludge addition from 5% to 30% at a sintering temperature of 1000^0C (Benlalla et al., 2015). Only few authors claimed the addition of sludge enhanced the mechanical performance of ceramic products up to 10% sludge replacement (Kizinievič et al., 2013). Apart from ceramic applications, DWTS has a potential as an alumino-siliceous substance to synthesize geopolymer (Geraldo et al., 2017; Nimwinya et al., 2016; Tang et al., 2019a). The results indicated that the addition of DWTS could delay setting time and degrade mechanical properties of geopolymer mortar (Geraldo et al., 2017; Nimwinya et al., 2016).

In addition, the feasibility of using DWTS as supplementary cementitious material and to produce lightweight aggregates was studied. However, the addition of sludge also deteriorated the mechanical and durability performance of concrete specimens regardless if used as a partial replacement of cementitious material or in the production of lightweight aggregates (El-Didamony et al., 2014; Hagemann et al., 2019; Huang and Wang, 2013; Huang et al., 2005).

More recently, several studies attempted to use oven-dried sludge at 105 ^{0}C for 24 hours into controlled low strength material (CLSM) (Fang et al., 2018; Wang et al., 2018a). This treatment method could be more environmentally friendly and energy conserving due to relatively low-temperature requirement and no additional emission of greenhouse gas. The authors reported that 12.5% sand replacement by DWTS decreased the compressive strength from 2.2 MPa to 0.6 MPa due to the fact that organic matter could form an isolation layer on the surface of calcium ions, affecting hydration reaction. Additionally, limited research was conducted to use wet DWTS to replace sand in concrete (Ramirez et al., 2017). The results indicated that the concrete mixture with 5% DWTS content could achieve 28-day

compressive strength of 28MPa. However, only limited information about durability performance was available. Furthermore, the micro-structure analysis and environmental impact of oven-dried DWTS in conventional concrete products has not been researched.

In this study, the feasibility of utilising DWTS in Concrete Paving Blocks (CPB) has been investigated. CPB can be manufactured by dry mix method with approximately zero slump of concrete mixture. The mechanical and durability properties of CPB with varying replacement ratios of sand by oven-dried DWTS were evaluated extensively. The following tests have been conducted and discussed, such as microstructure-chemical analyses, compressive strength, abrasion resistance, water absorption, sulfate attack, and toxic characteristic leaching procedure (TCLP).

92 # 2. Materials and experimental methods

93 ## 2.1 Materials

94 General Purpose (GP) cement based on AS 3972 (2010) was used as cementitious materials
95 for the production of the CPB. The aggregates used in this study were crushed stone, sand
96 and DWTS. The size of sand, provided by Sibelco Australia, was ranging from 8.68μm to
97 1.18mm with specific gravity of 2.61 and water absorption of 0.50%. The crushed stone,
98 sourced from Kulpara Quarry, was ranging from 2.06mm to 9.00mm, with specific gravity of
99 2.72 and water absorption of 1.17%.

100 The DWTS was collected from Happy Valley Water Treatment Plant (Fig. S1), which is
101 managed by SA Water and the largest water treatment facility (maximum treatment capacity:
102 100 megalitres/day) in South Australia. The DWTS disposed to landsite on 07/2016 was
103 chosen as research samples. The specific gravity and water absorption of DWTS were 2.27
104 and 28.82%, respectively, based on AS 1141.5 (2000). The moisture and organic matter
105 contents of DWTS specimen were 25% and 29.50% respectively, which were determined by
106 loss on ignition (LOI) test according to . The chemical components of DWTS were identified
107 by X-Ray Fluorescence (XRF) analysis (see Table 1). The results showed that Al_2O_3 and
108 organic matter constituted the major portion of the DWTS, followed by SiO_2, Fe_2O_3 and CaO.
109 Other oxides such as K_2O, MgO, CuO, TiO_2 and Na_2O were also observed. Referring to
110 Scanning electron microscopy (SEM) in Fig. 1a, the morphology of DWTS particles was
111 found to be irregular with particle sizes and porous structure. The X-ray diffraction (XRD)
112 revealed five major crystallizations were found in DWTS, including quartz (SiO_2), calcite
113 ($CaCO_3$), kaolinite ($Al_2Si_2O_5(OH)_2$), gypsum ($CaSO_4 \cdot 2H_2O$), and dolomite ($CaMg(CO_3)_2$)
114 (Fig. 1b). The Toxic Characteristic Leaching Procedure (TCLP) result of raw DWTS
115 indicated the leachability of Cu (1.8mg L^{-1}) exceeded the limitation of USEPA (1992) (1.3mg
116 L^{-1}). Thus, the leachability of CPB incorporating DWTS needs to be investigated.

Prior to mix, DWTS was screened with No. 12 sieve (1.68mm) and the particle size distribution of sand, crushed stone and DWTS was shown in Fig. 2, which indicated that no noticeable difference of the particle size between sand and DWTS can be detected, and that sand was slightly coarser than DWTS.

Table 1. Chemical compositions of DWTS.

Compositions	Weight percentage (wt%)
Al_2O_3	28.27
SiO_2	26.43
Fe_2O_3	6.66
CaO	5.36
K_2O	1.23
MgO	1.11
CuO	0.71
SO_3	0.48
LOI	29.5

(a)

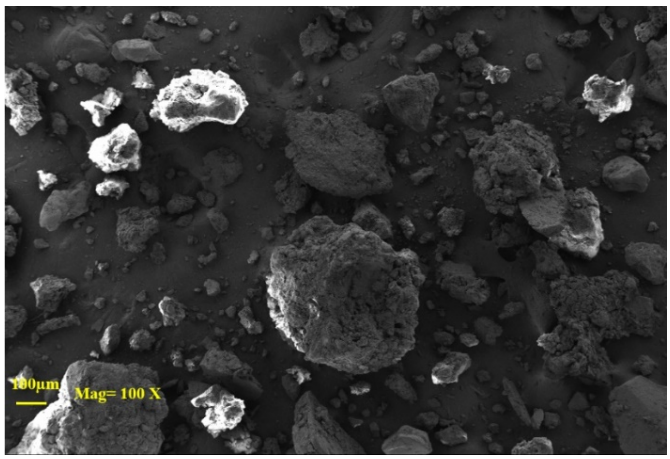

(b)

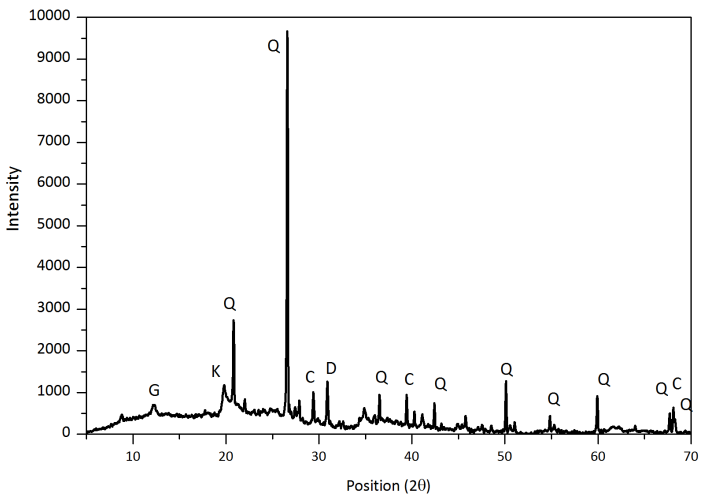

Fig. 1. SEM (a) and XRD spectra (b) of DWTS

(K: Kaolinite; Q: Quartz; G: Gypsum; D: Dolomite; C: Calcite).

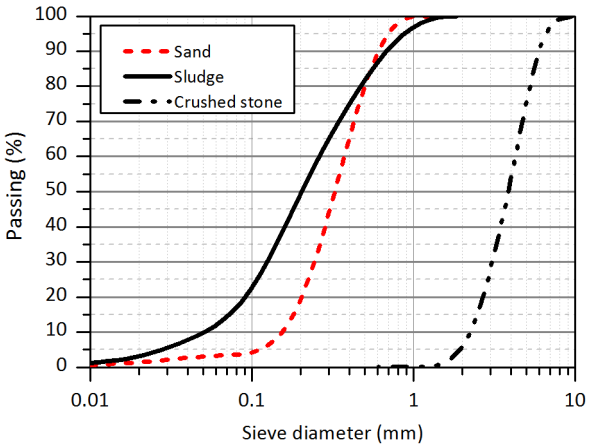

Fig. 2. Particle size distribution of sand, DWTS and crushed stone.

2.2 Mix proportion of CPB

A total of five mixes were prepared in the laboratory scale. Based on preliminary trials, the aggregate-to-cement ratio of 6.6 was used. In addition, the weight ratio of crushed stone to sand was kept at 1:1.3. The water/cement ratio was fixed at 0.3 for reference mix (CPB-0). Owing to the higher water absorption of DWTS, such ratios varied slightly with other mixes depending on different DWTS contents in CPB, namely 5%, 10%, 15%, and 20% corresponding to CPB-5, CPB-10, CPB-15, and CPB-20, respectively. Mix-proportion of CPB was provided in Table 2.

Table 2. Mix proportions of CPB with varying contents of DWTS (kg/m^3).

Mix notation	GP Cement	Concrete Sand	Crushed Stone	DWTS
CPB-0	299	851	1134	0
CPB-5	299	811	1134	42
CPB-10	299	767	1134	85
CPB-15	299	723	1134	129
CPB-20	299	682	1134	169

2.3 Manufacturing of CPB

CPB were produced by dry-mix method with the size of 115×115×50 mm^3 and aggregates (crushed stone, sand and DWTS) were oven dried at 105±3^{0}C for 24h before mix. For the mix, all dried ingredients were weighted and homogeneously mixed together for 1 minute. Water were then added to the mixtures before a further 3-minute mixing period. Load was applied slowly by a hydraulic compression machine and the pressure was fixed at 18MPa for 30s based on general industry practice. After carefully demoulding, all samples were covered by cling wrap and stored in a chamber at a constant temperature of 23 ±2^{0}C and relative humidity of 65% over 28-days curing period prior to carrying out the experimental testing . It should be noted that at least three replicates per mixture were produced for the following tests, except for leaching test where two samples were measured.

2.4 Test methods

2.4.1 Microstructural-chemical analyses

For SEM-based microstructural analysis, small pieces of crushed CPB taken from 2 to 4mm sample depth were oven-dried at 40^{0}C for 48h and then carbon-coated. In order to detect sludge, sand and other crystallizations, Energy Dispersive X-ray spectroscopy (EDS) helped to identify chemical elements. The crystalline phases of crushed CPB samples were determined by X-ray Diffractometry (XRD). A representative pieces of CPB obtained from similar position of the samples used for SEM analysis were ground to minus 30μm. XRD was conducted using CuKα radiation at 40kV and 40mA. The scan angle was between 5^{0}C and 70^{0}C at the scan speed of 0.2°/min.

161 2.4.2 Compressive test

162 Compressive strength of CPB was determined in accordance with AS 4456.4 (2003). The
163 specimen was compressed by the universal testing machine with the wearing face up. The
164 load was applied at a constant rate of 0.150MPa/s, without any shock, until failure.

165 2.4.3 Abrasion resistance test

166 The abrasion resistance test was set up in accordance to AS 4456.9 (2003). It involved
167 securing the specimens to a tumbling machine with the inward faces of the specimens placed
168 over holes on the outside of the tumbling drum. Six hundred steel balls were placed within
169 the drum and the tumbling machine ran for 3600 revolutions at a speed of 60 rotations per
170 minute. After the test, the samples were immersed in potable water at least 2 hours and then
171 weighed in water and in saturated surface dry condition to get the bulk density of samples. To
172 eliminate the atmosphere effect for this test, two samples were selected randomly from 18
173 CPB samples as control specimens. The mass loss and abrasion index were calculated
174 according to Eq. 1-3, respectively.

175 $$\text{Mass loss (\%)} = \frac{m_1 - m_2}{m_1} \times 100 \quad (1)$$

176 $$\text{Abrasion index} = \frac{m_1 - (m_2 - C)}{B_d} \times 10^3 \quad (2)$$

177 $$B_d = \text{bulk density} = \left(\frac{m_2}{m_3 - m_4}\right) \times \rho \ \ and \ \ C = m_5 - m_6 \quad (3)$$

178 Where, m_1 is the initial weight of test sample (g); m_2 is the weight of test sample after test
179 (g); m_3 and m_4 are the weight of specimens after immersing in water and under water,
180 respectively (g); m_5 and m_6 are the weight of control samples before and after test (g); C is
181 the correction (g); B_d is the bulk density (kg/m^3); ρ is the density of water (kg/m^3).

182 2.4.4 Water absorption test

183 According to AS 4456.14 (2003), CPB samples were oven dried at 110±8 ^{0}C until a constant
184 weight, before fully immersing in cold potable water for 24 h. The saturated CPB specimens
185 were then dried with a damp cloth to remove surface water and finally weighted. The water
186 absorption of CPB was calculated by Eq. 4, where m_1 is the mass of dried sample and m_2 is
187 the mass of immersed surface dried sample (g).

188 $$Water\ absorption\ (\%) = \frac{(m_2 - m_1)}{m_1} \times 100 \quad (4)$$

189 2.4.5 Sodium sulfate attack test

190 There are some measurement methods to assess the resistivity of concrete products to sodium
191 sulfate attack, such as weight loss, ultrasonic pulse velocity (UPV), compressive strength,
192 expansion, damage variable, and visual appearance (Jiang and Niu, 2016; Nehdi et al., 2014;
193 Pham et al., 2019; Scherer, 2004; Sotiriadis et al., 2012; Tang et al., 2019b; Yu et al., 2013).
194 In this study, visual appearance, weight loss, and UPV of CPB were studied as the indicators
195 of resistance of CPB to sodium sulfate attack.

196 The resistance to sulfate attack test of CPB samples was carried out according to AS 4456.10
197 (2003). The sulfate solution was prepared by dissolving 62 g Na_2SO_4 in 1L of distilled water.
198 Each cycle of this test started by immersing the specimens in sulfate solution for 2 h and then
199 oven dried at 65±3 ^{0}C for 20±1 h. During the test, pH value of solidum sulfate solution was
200 maintained between 6-8. The mass and UPV of CPB samples were measured after cooling
201 the specimens to room temperature (2±0.5 h). The test was repeated with above steps for 17
202 cycles. The mass loss (%) was determined by Eq. 5, where m_0 and m_i are weights before
203 starting test and after ith cycle of sulfate attack (g), respectively. The UPV was measured
204 based on ASTM C597 (2016) and the frequency of generated ultrasonic pules was 54kHz.

205 UPV (m/s) is calculated by Eq. 6, where L is path length of pulse travel (m) and t is the
206 measured time (s).

207 $$\text{Mass loss}\ (\%) = \frac{m_0 - m_i}{m_0} \times 100 \quad (5)$$

208 $$\text{UPV}\ (m/s) = \frac{L}{\mathrm{t}} \quad (6)$$

209 2.4.6 Toxic characteristic leaching procedure (TCLP)

210 Due to the hazardous leaching problem of raw DWTS discussed in section 2.1, TCLP was
211 conducted for CPB. The leachability of metal elements was the main concern for applications
212 of DWTS in CPB. According to the USEPA (1992), the crushed samples were taken from the
213 specimens after compressive strength tests and were screened by a 10mm sieve. For each
214 CPB, 20 g of crushed sample was put into 400mL of the TCLP leachate (5.7mL of glacial
215 acetic acid in 2 L of distilled water) and then shaken for 18 h on an automatic shaker (Ling
216 and Poon, 2014). The concentration of different metals in the leachate was determined by
217 Agilent 8800 Inductively Coupled Plasma Mass Spectrometry (ICP-MS).

218

219 # 3. Results and discussion

220 ## 3.1. Microstructural chemical characterizations

221 ### 3.1.1. Microstructural observations

222 Fig. 3a shows the SEM images of CPB with DWTS content varying from 0% to 15%. The
223 dominated compound in CPB-0 was the cotton-shaped C-S-H (calcium silicate hydrate) gel,
224 which was the main hydration product of Portland cement. A similar microstructure to CPB-0
225 was also observed on CPB-5. For CPB-10, the C-S-H gel was not evenly distributed
226 compared with CPB-0. Needle-shaped ettringite was also revealed on CPB-10 and especially
227 more visible on CPB-15. However, the cotton-shaped C-S-H gel was not visible in CPB-15.

On one hand, the difference in SEM images of CPB samples with higher contents of DWTS could be due to the organic matter in DWTS which hindered the formation of portlandite and C-S-H gel (Wang et al., 2018b). On the other hand, it could be due to the chemical composition of DWTS, which contained alum and gypsum. Initially, the Ca^{2+} ions from portlandite or gypsum dissolved in solution reacted with C_3A and sulfate ions to form ettringite. Furthermore, the sulfates reacted with the monosulfate and Ca^{2+} ions to produce more ettringite, where Ca^{2+} was provided by CH or C-S-H after depletion of CH (Menéndez et al., 2013).

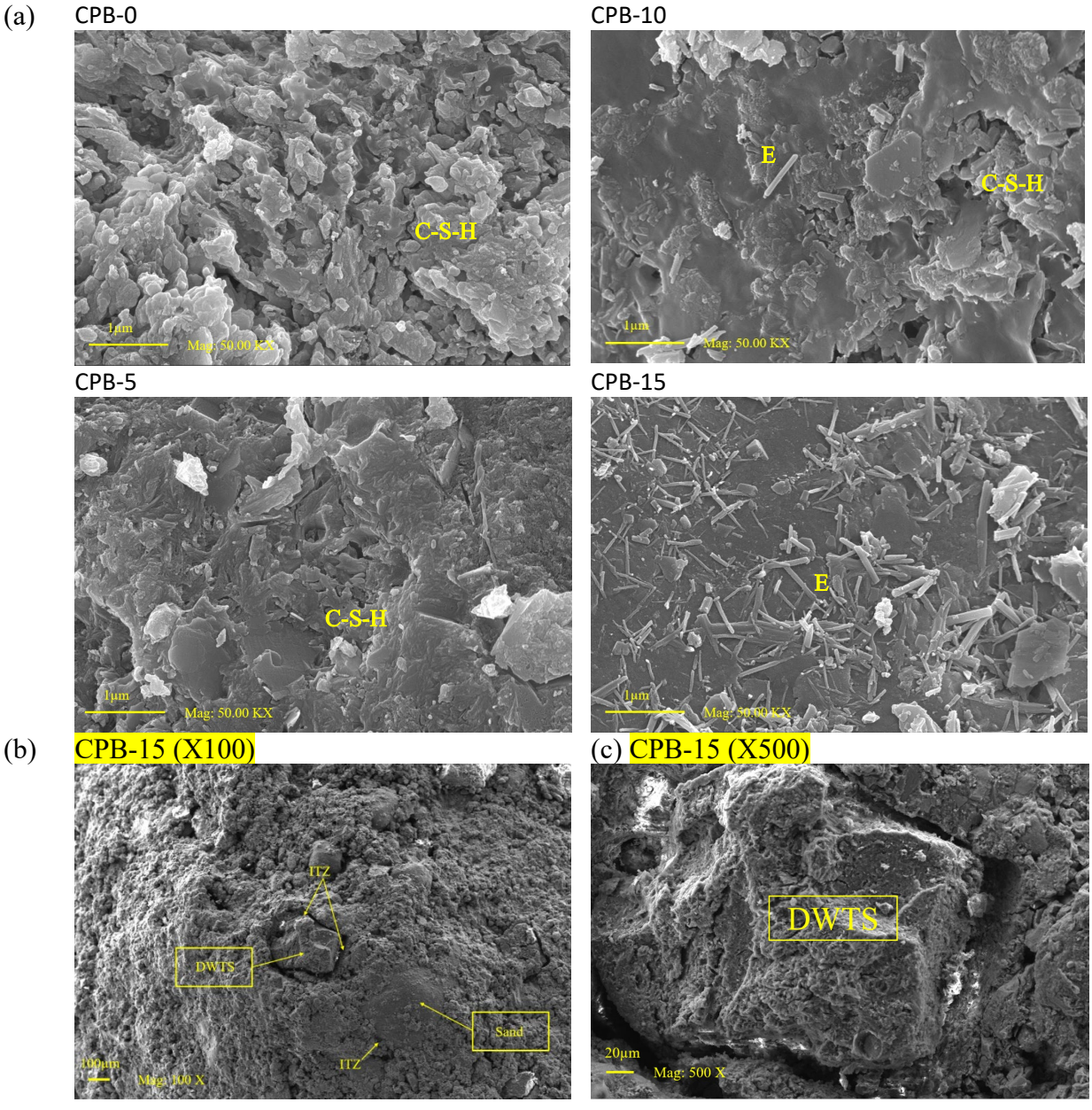

(d)

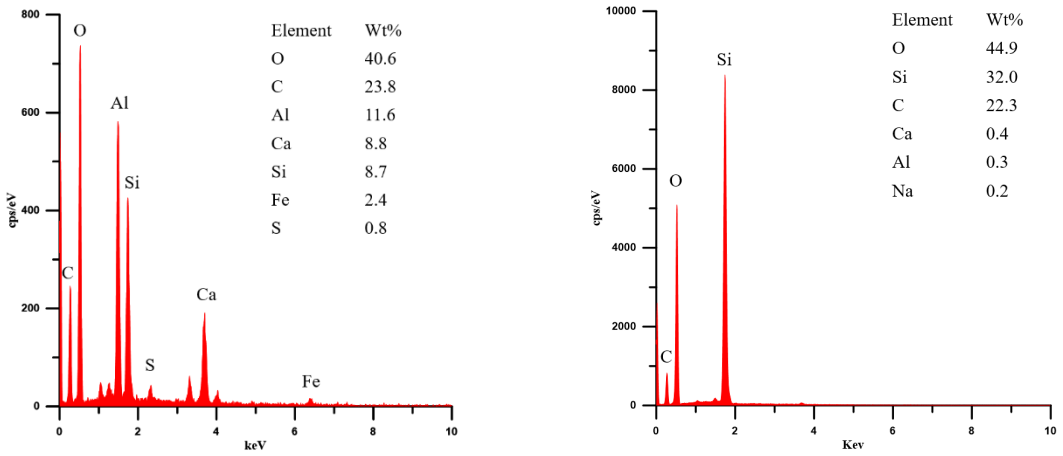

Fig. 3. SEM-EDS analysis of CPB (a) SEM images of CPB with varying contents of DWTS (CSH: Calcium-Silicate-Hydrate; E: Ettringite), (b) ITZ between aggregates (sand and DWTS) and cement matrix (100X) in CPB-15, (c) ITZ between DWTS and cement matrix (500X) in CPB-15, (d) EDS analysis for DWTS and sand.

It is well known that the strength of concrete is affected by strength of cement matrix, aggregates, and the interfacial transition zone (ITZ) between cement matrix and aggregates. ITZ has been recognized as the weakest phase in concrete and the denser and smaller thickness of ITZ indicate a stronger interfacial bonding between aggregate and cement matrix (Poon et al., 2004). Fig. 3b and 3c shows the interfaces of cement-DWTS and cement-sand in CPB samples. Fig. 3d identified the substance of corresponding areas by EDS, which showed DWTS and sand, respectively. Generally, the DWTS-cement interfaces observed from SEM images were very loose, and the thickness of ITZ was varying along the surface of DWTS, approximately between 30-40µm (Fig. 3b). Fig. 3c shows a higher magnification of DWTS-cement interface, it exhibits the ITZ is porous and some loose particles stockpiles in this area.

It can be explained by the high-water absorption capacity of DWTS, which absorbs a large amount of water, resulting in lack of free water for cement hydration. Thus, the wider and more porous ITZ was observed in hardened CPB incorporating DWTS. Compared with DWTS, the sand-cement interface was relatively denser with maximum thickness around 15µm (see Fig. 3b).

255 3.1.2 Composition analysis

256 Fig. 4 shows the XRD spectra of CBP with 0%, 5%, 10% and 15% DWTS contents. For the
257 reference specimens (CPB-0), obvious diffraction peaks for CH, and quartz and dolomite
258 could be observed. CPB-5 exhibited similar diffraction pattern to CPB-0, except for the
259 presence of gypsum, which could be derived from DWTS. Compared with CPB-5 and CPB-0,
260 CH proportion was significantly reduced and some diffraction peaks of ettringite were
261 observed in the CPB-10. Furthermore, CH peaks were noticeably diminished in CPB-15.
262 Instead, a significant increase in the peak intensity of CPB-15 at 32.3^{0}C associated with two
263 over lapping peaks of C_2S and C_3S were observed. It confirmed the addition of DWTS may
264 hinder the cement hydration. In addition, the diffraction peaks of ettringite in CPB-15 was
265 higher than that of CPB-10, which proved large content of DWTS could result in formation
266 of ettringite. The peak of gypsum in CPB-15 was not as clear as CPB-10 and CPB-5,
267 attributing to the formation of ettringite consumed gypsum.

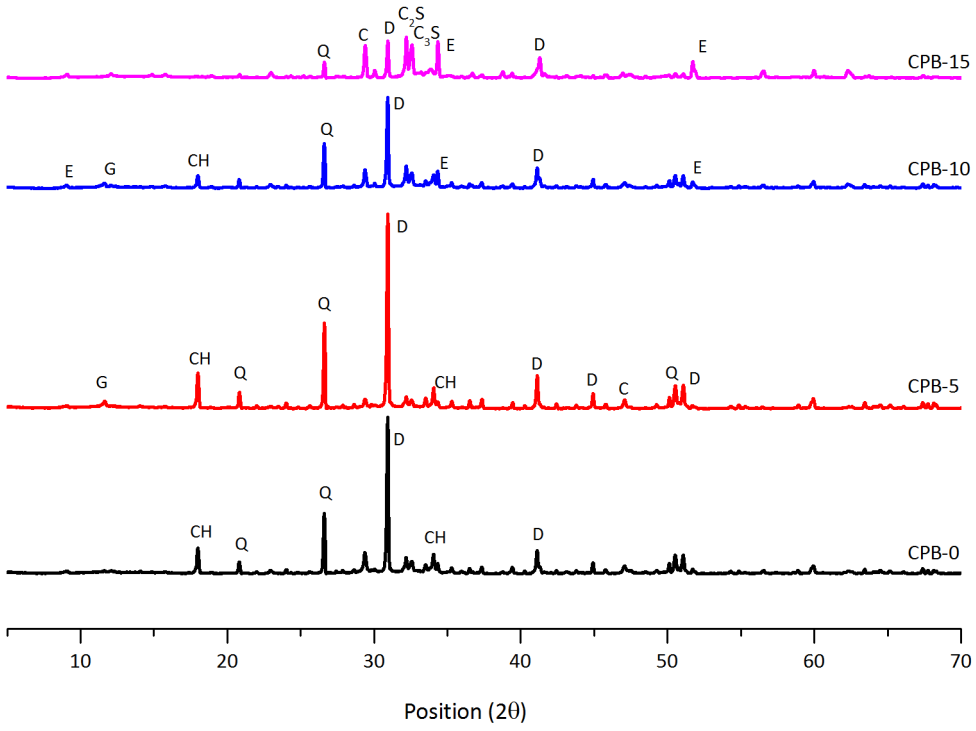

268

269 Fig. 4. XRD spectra of CPB with varying contents of DWTS (Q: Quartz; C: Calcite; E: Ettringite; D: Dolomite;
270 G: Gypsum; CH: Portlandite; C_2S: Dicalcium silicate; C_3S: Tricalcium silicate).

3.2 Mechanical and durability properties

3.2.1 Compressive strength

Table 3 shows the compressive strength of five mixes at 28-days of curing. The compressive strengths of CPB with 0%, 5%, 10%, 15% and 20% contents of DWTS were 48.69MPa, 52.20MPa, 43.25MPa, 9.92MPa and 4.13MPa, respectively. The compressive strength of CPB-5 was comparable with the control mix (CPB-0). However, compared to CPB-0, the compressive strengths of CPB-10, CPB-15, and CPB-20 were lower, namely 11.2%, 79.6%, and 91.5%, respectively. The strength requirement of CPB in Australia was 43MPa (Ghafoori and Smith, 1992). Thus, the obtained results indicated the maximum replacement ratio of sand by DWTS in CPB was 10%.

The adverse effect of incorporating DWTS on compressive strength can be attributed to the loss of cohesion between DWTS and cement matrix as observed in Fig 3 and hindering of cement hydration. The DWTS was characterised with high-water absorption rate and high content of organic matter. The increased DWTS content in CPB could result in lack of water for cement hydration, since a larger amount of free water was absorbed by oven-dried DWTS. In addition, the organic matter contained in DWTS (29.5%) hindered the formation of hydration products (Wang et al., 2018a). Thus, the deterioration of CPB was getting more severe with the increasing of DWTS replacement levels. Eventually, the strength development of CPB with 20% untreated DWTS content was almost invisible.

3.2.2 Abrasion resistance

Due to completed disintegration of CPB-15 and CPB-20 within 15 minutes from the start of the experiment, the test results only include CPB-0, CPB-5, and CPB-10. The effect of addition of DWTS on abrasion resistance of CPB is shown in Table 3. The average abrasion

296 index for CPB-0, CPB-5, and CPB-10 were 11.91, 12.23, 12.42, respectively. The results
297 confirmed that the addition of DWTS up to 10% had no significant effect on the resistance of
298 CPB to abrasion, which can be related to the relatively good strength of CPB-0, CPB-5 and
299 CPB-10 and good compatibility of DWTS in CPB under 10% replacement level.

300 **Table 3.** Strength and durability properties of CPB with varying contents of DWTS.

Mix notation	Compressive strength (MPa)	Abrasion properties			Water absorption (%)
		Mass loss (%)	Abrasion Index	Notes	
CPB-0	48.69(±2.3)	1.9(±0.1)	11.91(±0.32)		4.2(±0.35)
CPB-5	52.20(±1.9)	1.6(±0.2)	12.23(±0.52)		3.8(±0.15)
CPB-10	43.25(±2.2)	2.1(±0.2)	12.42(±0.56)		5.1(±0.25)
CPB-15	9.92(±1.4)	-	-	Specimens failed	7.3(±0.20)
CPB-20	4.13(±0.8)	-	-	Specimens failed	7.7(±0.15)

301

302 3.2.3 Water absorption

303 The water absorption of the five DWTS contents at 28-days are shown in Table 3. It can be
304 seen that the water absorption of CPB with 0%, 5%, 10%, 15%, and 20% DWTS replacement
305 were 4.2%, 3.8%, 5.1%, 7.3% and 7.7%, respectively. The CPB-0, CPB-5 and CPB-10
306 demonstrated relative low water-absorption. The CPB with 15% and 20% DWTS
307 replacements did not satisfy the criteria for water absorption (less than 6%) (Jankovic et al.,
308 2012). Generally, the water absorption of CPB increased with the addition of DWTS. This
309 can be explained by the porous structure of CPB incorporating DWTS which resulted in
310 higher water absorption. However, the CPB with 5% DWTS content demonstrated a denser
311 structure, which resulted in lower water-absorption ability.

312 3.2.4 Sulfate attack

313 3.2.4.1 Mass loss

314 Fig. 5a shows the mass loss of CPB with the five DWTS contents. The increase in mass for
315 CPB with DWTS contents of 0%, 5%, and 10% were 3.2%, 3.8%, and 3.2% after 17 cycles

316 of salt attack, respectively. The mass of CPB-15 and CPB-20 both started to decrease at the
317 7^{th} cycle, and the final mass losses were 10.72% and 11.69%, respectively. Furthermore, the
318 reduction rate in the mass of CPB-20 was slightly higher than CPB-15.

319 Due to wetting and drying cycles in experimental process, the deterioration of CPB samples
320 could be from a combination of physical and chemical attack. For instance, the sodium
321 sulfate solution could be absorbed by capillary suction and the subsequent evaporation of
322 water could contribute to the deposit of salt in pores close to surface of CPB (Scherer,
323 2004).The chemical attack was characterized by chemical reactions between sulfate and
324 aluminate components in hardened cement pastes to produce expansive ettringite and gypsum,
325 leading to loss of concrete pieces (Bakhareva et al., 2002).

326 The increase in weight associated with CPB-0, CPB-5 and CPB-10 could be attributed to the
327 gradual infiltration of sulfate solution into the capillary voids of CPB and the consequent
328 reaction with alumina-containing hydrates forms ettringite. The formed ettringite can fill the
329 voids of the composite matrix and result in the increase of mass. For the significant weight
330 loss of CPB-15 and CPB-20, it can be explained by the porous structure of DWTS and the
331 high contents of DWTS. Compared with CPB-0, CPB-5, and CPB-10, the pavers
332 incorporating higher sludge contents (15% and 20%) with more porous microstructure were
333 easier to be penetrated by the salt solution and higher aluminium content was detrimental to
334 sulfate resistance (Bakhareva et al., 2002). The excessive formation of ettringite caused
335 tensile stresses to develop, leading to crack initiation and CPB deterioration when such
336 stresses became greater than the tensile strength of the composites (Pham et al., 2019). In
337 addition, the accumulation of salt crystallization during the wetting cycle could cause spalling
338 and cracking due to the thenardite reprecipitating as mirabilite (Scherer, 2004).

Fig. 6 presents the images of typical specimens with DWTS content from 0 to 20% after 17 cycles of salt attack. Minor spalling of surface skin was evident on the corner and edges of CPB-0, CPB-5 and CPB-10. For CPB-15 and CPB-20, the surface spalling was much more serious than CPB-0, CPB-5 and CPB-10. No cracking was noticed in all mixtures. Only CPB-0, CPB-5, and CPB-10 can meet the requirements of AS 4455.2 (2010), which specified the maximum weight loss should not exceed 0.4g after 17 cycles of the experiment.

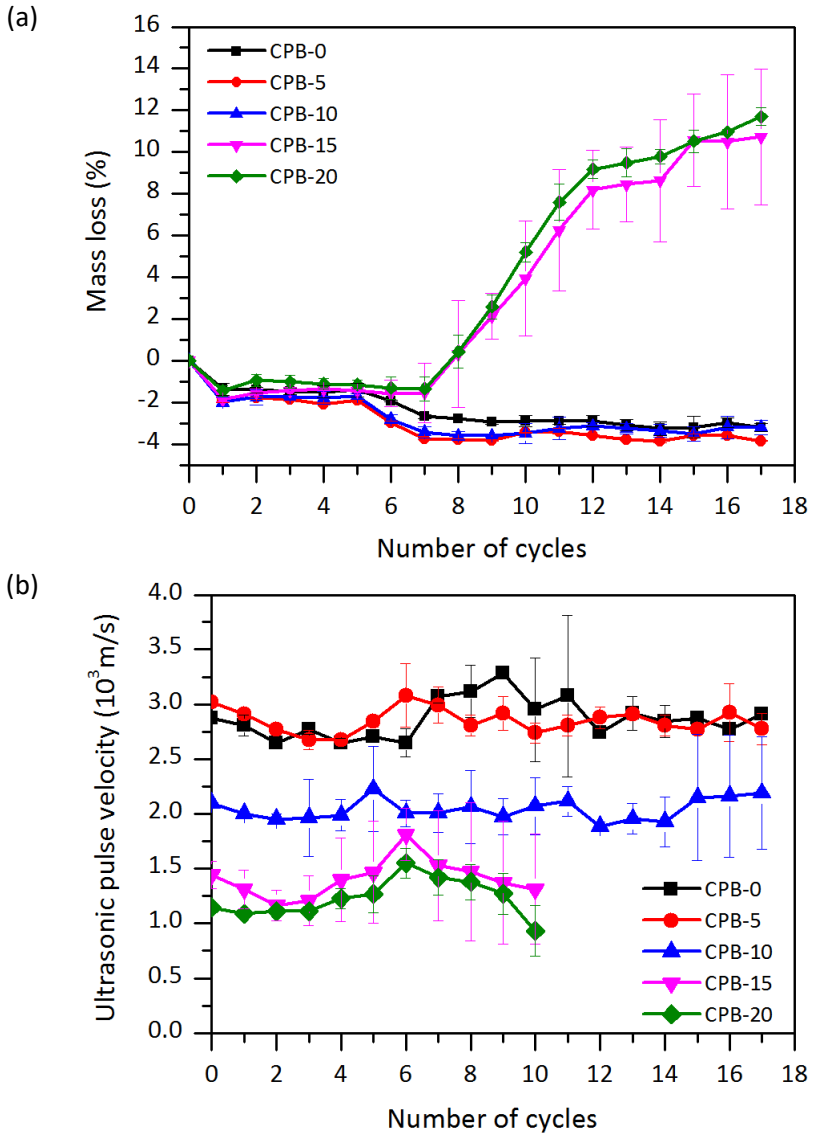

Fig. 5. Mass loss (a) and change of ultrasonic pulse velocity (b) with varying replacement ratios of DWTS.

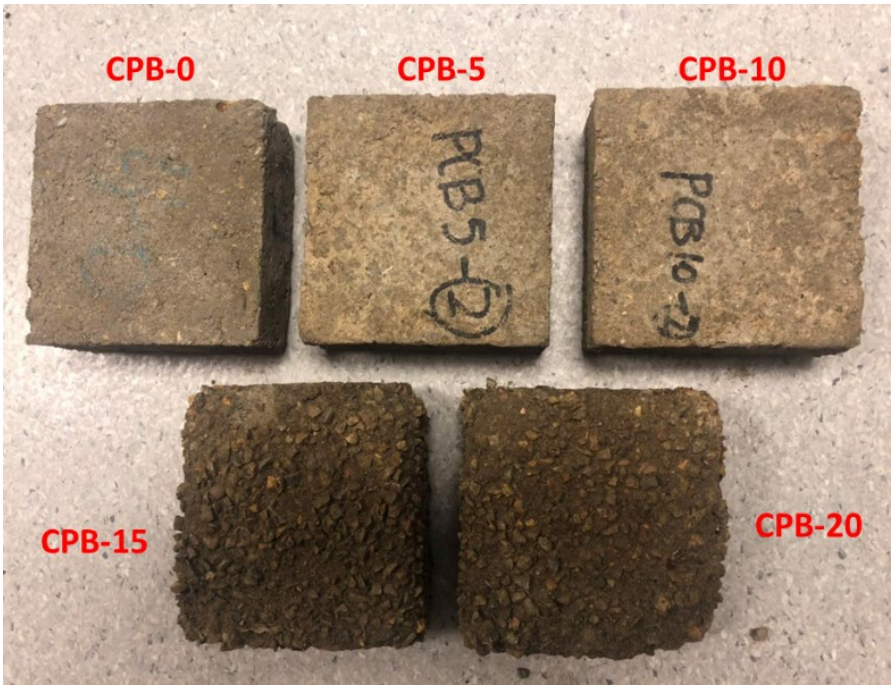

Fig. 6. Degradation of CPB samples after 17 cycles of salt attack.

3.2.4.2 Ultrasonic pulse velocity (UPV)

UPV is a non-destructive test method, which can detect the interior of the specimen and provide evidence of the micro-crack inside concrete block (Tang et al., 2019b). The UPV of CPB over 17 cycles of sulfate attack is shown in Fig. 5b. Note that, due to severe deterioration of CPB surface exposed to sulfate attack, the velocity measurement for CPB-15 and CPB-20 were only carried out for the first ten cycles. The initial UPV of CPB-5 was quite identical to CPB-0. This was attributed to the similar dense micro-structure which reduced transmitting time of ultrasonic pulse waves, leading to the higher pulse velocity. Under the condition of sodium sulfate attack, pulse velocities of CPB-0, CPB-5, and CPB-10 had no significant change compared with their original values. On the other hand, CPB-15 and CPB-20 exhibited a higher rate of velocity increase at 6^{th} cycle due to the formation of ettringite, which helped to densify the microstructure of composite. However, the extreme development of the expansive product resulted in cracks and consequently the UPV was significantly decreased until fractured.

3.3 Toxic characteristic leaching procedure

Table 4 reports the leaching behaviour of raw DWTS and CPB with varying DWTS contents. The results indicated that the leaching concentrations of the listed elements of CPB with varying DWTS contents were low, and all the detected heavy metals were within the limitation based on (USEPA, 1992).

The leaching rate of the CPB was mainly controlled by capillary diffusion. During the immersing process, water penetrated into the CPB due to the existence of capillary voids, therefore chemical elements can dissolve into water. When water attained the potential maximum depth gradually, the elemental leaching rate was decreased significantly, and the leaching concentrations of elements appeared to be stable. Thus, the leaching concentrations of Al and Cu generally increased with the increase of DWTS contents from 5% to 20% in CPB, which allowed water to be transported quicker due to the higher porosity of the composites. The obtained results indicated that the cement-based material was efficient to immobilise metal elements and the addition of DWTS into CPB was safe.

Table 4. Leachate concentration of DWTS and CPB samples (mg L^{-1}).

Samples	Al	Cr	Mn	Ni	Cu	Zn	As	Ba	Pb	Cd
DWTS	51.504	0.003	4.222	0.022	1.810	0.063	0.006	0.580	0.002	0.001
CPB-5	0.057	0.035	0.520	0.024	0.020	0.062	0.002	0.196	0	0
CPB-10	0.121	0.042	0.334	0.021	0.030	0.032	0.001	0.032	0	0
CPB-15	0.944	0.046	0.776	0.024	0.081	0.063	0.001	0.063	0.002	0
CPB-20	2.136	0.046	0.494	0.019	0.125	0.080	0.002	0.080	0.002	0.001
Regulatory Limits	-	0.6	-	-	1.3	4.3	10.2	-	0.75	1.53

4. Conclusions

This study aimed to explore the potential possibility of adding DWTS into CPB as a replacement for sand. The experimental results proved that DWTS can be used to replace fine aggregates and the maximum DWTS contents in CPB could be up to 10% depending on paving criteria. From the analysis of experimental results, some conclusions can be drawn:

(1) The microstructural analysis revealed high porosity of CPB with DWTS incorporation, especially at the ITZ between DWTS and cement matrix. Ettringite was also formed in the composites incorporating high DWTS content due to sulfur and alum available in DWTS.

(2) CPB exhibited a reduction in 28-day compressive strength with increasing of DWTS content, except for CPB with 5% DWTS. The strength decreased significantly when higher DWTS contents were used (15% and 20%) due to a more porous structure and higher organic matter in DWTS.

(3) The increasing content of DWTS was detrimental to abrasion resistance and increased water absorption of CPB. CPB with above 10% of DWTS did not satisfy the requirement for water absorption of pavers and also was damaged quickly after starting the abrasion test.

(4) For the durability of pavers under aggressive environments, CPB incorporating up to 10% of DWTS could maintain the resistance of the composites to sodium sulfate attack as reference mix (CPB-0). Severe spalling was observed on CPB with higher DWTS content due to both chemical and physical sodium sulfate attack.

(5) In spite of the high leachability of Cu in DWTS used, this element and all the other metals in DWTS were well immobilised in CPB, so the obtained product was non-hazardous for paving application.

Acknowledgements

The authors would like to acknowledge UniSA and SA Water for the research scholarship and financial support of this project.

6. References

Ahmad, T., Ahmad, K., Alam, M., 2016. Sustainable management of water treatment sludge through 3'R' concept. Journal of Cleaner Production 124, 1-13.

Anderson, M., Biggs, A., Winters.C, 2003. Use of two blended water industry by-product wastes as a composite substitute for traditional raw materials used in clay brick manufacture, Recycling and Reuse of Waste Materials. Thomas Telford Publishing, pp. 417-426.

AS 1141.5, 2000. Particle density and water absorption of fine aggregate. Standards Australia.

AS 3972, 2010. General purpose and blended cements. Standards Australia.

AS 4455.2, 2010. Masonry units, pavers, flags and segmental retaining wall units. Standards Australia.

AS 4456.4, 2003. Determining compressive strength of masonry units. Standards Australia.

AS 4456.9, 2003. Determing abraision resistance. Standards Australia.

AS 4456.10, 2003. Determing resistance to salt attack. Standards Australia.

AS 4456.14, 2003. Determining water absorption properties. Standards Australia.

ASTM C597, 2016. Standard Test Method for Pulse Velocity through Concrete, ASTM International, West Conshohocken, PA.

Babatunde, A.O., Zhao, Y.Q., 2007. Constructive Approaches Toward Water Treatment Works Sludge Management: An International Review of Beneficial Reuses. Critical Reviews in Environmental Science and Technology 37, 129-164.

Bakhareva, T., Sanjayana, J.G., Cheng, Y.-B., 2002. Sulfate attack on alkali-activated slag concrete. Cement and Concrete Research 32, 211-216.

Benlalla, A., Elmoussaouiti, M., Dahhou, M., Assafi, M., 2015. Utilization of water treatment plant sludge in structural ceramics bricks. Applied Clay Science 118, 171-177.

De Carvalho Gomes, S., Zhou, J.L., Li, W., Long, G., 2019. Progress in manufacture and properties of construction materials incorporating water treatment sludge: A review. Resources, Conservation and Recycling 145, 148-159.

El-Didamony, H., Khalil, K.A., Heikal, M., 2014. Physico-chemical and surface characteristics of some granulated slag–fired drinking water sludge composite cement pastes. Housing and Building National Research Center Journal 10, 73-81.

Fang, X., Wang, L., Poon, C.S., Baek, K., Tsang, D.C.W., Kwok, S.K., 2018. Transforming waterworks sludge into controlled low-strength material: Bench-scale optimization and field test validation. Journal of Environmental Management 232, 254-263.

Geraldo, R.H., Fernandes, L.F.R., Camarini, G., 2017. Water treatment sludge and rice husk ash to sustainable geopolymer production. Journal of Cleaner Production 149, 146-155.

Hagemann, S.E., Gastaldini, A.L.G., Cocco, M., Jahn, S.L., Terra, L.M., 2019. Synergic effects of the substitution of Portland cement for water treatment plant sludge ash and ground limestone: Technical and economic evaluation. Journal of Cleaner Production 214, 916-926.

Huang, C.-H., Wang, S.-Y., 2013. Application of water treatment sludge in the manufacturing of lightweight aggregate. Construction and Building Materials 43, 174-183.

Huang, C., Pan, J.R., Liu, Y., 2005. Mixing Water Treatment Residual with Excavation Waste Soil in Brick and Artificial Aggregate Making. Journal of Environmental Engineering 131, 272-277.

Huang, C., Pan, J.R., Sun, K.-D., Liaw, C.-T., 2001. Reuse of water treatment plant sludge and dam sediment in brick-making. Water Science and Technology 44, 273-277.

Jankovic, K., Nikolic, D., Bojovic, D., 2012. Concrete paving blocks and flags made with crushed brick as aggregate. Construction and Building Materials 28, 659-663.

Jiang, L., Niu, D., 2016. Study of deterioration of concrete exposed to different types of sulfate solutions under drying-wetting cycles. Construction and Building Materials 117, 88-98.

Keeley, J., Jarvis, P., Judd, S.J., 2014. Coagulant Recovery from Water Treatment Residuals: A Review of Applicable Technologies. Critical Reviews in Environmental Science and Technology 44, 2675-2719.

Kizinievič, O., Žurauskienė, R., Kizinievič, V., Žurauskas, R., 2013. Utilisation of sludge waste from water treatment for ceramic products. Construction and Building Materials 41, 464-473.
Ling, T.-C., Poon, C.-S., 2014. Use of recycled CRT funnel glass as fine aggregate in dry-mixed concrete paving blocks. Journal of Cleaner Production 68, 209-215.
Ling, Y.P., Tham, R.-H., Lim, S.-M., Fahim, M., Ooi, C.-H., Krishnan, P., Matsumoto, A., Yeoh, F.-Y., 2017. Evaluation and reutilization of water sludge from fresh water processing plant as a green clay substituent. Applied Clay Science 143, 300-306.
Maiden, P., Hearn, M., T,W., Boysen, R.I.C., P. , Warnecke, 2015. Alum Sludge Re-Use, Investigation (10OS-42) Prepared by GHD and Centre for Green Chemistry (Monash University) for The Smart Water Fund, Victoria, ACTEW Water & Seawater, Melbourne, Australia.
Menéndez, E., Matschei, T., Glasser, F.P., 2013. Sulfate Attack of Concrete in Performance of Cement-Based Materials in Aggressive Aqueous Environments. Springer.
Nehdi, M.L., Suleiman, A.R., Soliman, A.M., 2014. Investigation of concrete exposed to dual sulfate attack. Cement and Concrete Research 64, 42-53.
Nimwinya, E., Arjharn, W., Horpibulsuk, S., Phoo-ngernkham, T., Poowancum, A., 2016. A sustainable calcined water treatment sludge and rice husk ash geopolymer. Journal of Cleaner Production 119, 128-134.
Pham, N.P., Toumi, A., Turatsinze, A., 2019. Evaluating damage of rubberized cement-based composites under aggressive environments. Construction and Building Materials 217, 234-241.
Poon, C.S., Shui, Z.H., Lam, L., Fok, H., Kou, S.C., 2004. Influence of moisture states of natural and recycled aggregates on the slump and compressive strength of concrete. Cement and Concrete Research 34, 31-36.
Ramirez, K.G., Possan, E., Dezen, B.G.d.S., Colombo, M., 2017. Potential uses of waste sludge in concrete production. Management of Environmental Quality: An International Journal 28, 821-838.
Sarabia, A., Sanchez, J., Sanchez, J.V., 2019. Effect of the incorporation of residual sludge from water treatment on the technological properties of ceramic bodies: A review. Journal of Physics: Conference Series 1388.
Scherer, G.W., 2004. Stress from crystallization of salt. Cement and Concrete Research 34, 1613-1624.
Sotiriadis, K., Nikolopoulou, E., Tsivilis, S., 2012. Sulfate resistance of limestone cement concrete exposed to combined chloride and sulfate environment at low temperature. Cement and Concrete Composites 34, 903-910.
Tang, Z., Li, W., Hu, Y., Zhou, J.L., Tam, V.W.Y., 2019a. Review on designs and properties of multifunctional alkali-activated materials (AAMs). Construction and Building Materials 200, 474-489.
Tang, Z., Li, W., Ke, G., Zhou, J.L., Tam, V.W.Y., 2019b. Sulfate attack resistance of sustainable concrete incorporating various industrial solid wastes. Journal of Cleaner Production 218, 810-822.
USEPA, 1992. Toxicity Characteristic Leaching Procedure, U.S. Environmental Protection Agency. Washington, DC, USA, 1992.
Wang, L., Chen, L., Tsang, D.C.W., Li, J.-S., Baek, K., Hou, D., Ding, S., Poon, C.-S., 2018b. Recycling dredged sediment into fill materials, partition blocks, and paving blocks: Technical and economic assessment. Journal of Cleaner Production 199, 69-76.
Wang, L., Zou, F., Fang, X., Tsang, D.C.W., Poon, C.S., Leng, Z., Baek, K., 2018a. A novel type of controlled low strength material derived from alum sludge and green materials. Construction and Building Materials 165, 792-800.
Wolff, E., Schwabe, W.K., Conceição, S.V., 2015. Utilization of water treatment plant sludge in structural ceramics. Journal of Cleaner Production 96, 282-289.
Yu, C., Sun, W., Scrivener, K., 2013. Mechanism of expansion of mortars immersed in sodium sulfate solutions. Cement and Concrete Research 43, 105-111.